Arab J Sci Eng (2018) 43:1383–1394
https://doi.org/10.1007/s13369-017-2872-9

RESEARCH ARTICLE - MECHANICAL ENGINEERING

Microstructural Characterization, Mechanical, Physical and Thermal Properties of a Diesel Particulate Filter

Nurcan Calis Acikbas[1] · Yigit Ture[1] · Emre Gurlek[2] · Selcuk Ozcan[3] · Seref Soylu[2] · Gokhan Acikbas[4] · Turker Gudu[5]

Received: 6 July 2017 / Accepted: 6 October 2017 / Published online: 3 November 2017

Abstract In the literature, limited studies are available due to the challenges of the detailed microstructural characterization and determination of properties of diesel particulate filters (DPFs). For this reason, the characterization of a commercial DPF was carried out with different techniques with the aim to identify the manufacturing processes, the chemical composition, the microstructure and the mechanical, physical and thermal properties. Scanning electron microscopy (energy-dispersive X-ray spectroscopy, back-scattered electron, secondary electron detectors), X-ray diffraction, universal mechanical testing, Archimedes technique, dilatometer and C-therm thermal conductivity analysis tools were used for the characterization. During DPF regeneration, the tailoring of these properties has crucial effect on the reliability and durability of the filter. The value of the thermal shock resistance parameter group $\sigma_f/E\alpha$ was calculated to be 426 K, while thermal conductivity (k) was determined as 1.95 W/mK. When compared to the literature values for dense SiC, the $\sigma_f/E\alpha$ value indicated a better thermal shock resistance; however, thermal conductivity was on the limits of an order of magnitude worsening the thermal shock resistance. Therefore, to improve the thermal shock resistance of the filter material, the thermal conductivity value has to be increased to the maximum allowed by the required porosity. The study may lead to tailoring of an optimized SiC DPF material.

Keywords SiC filter · Characterization · Microstructure · Thermal properties · Diesel particle filter · Porous materials

1 Introduction

Diesel engines have been preferred power sources for heavy duty applications due to their superior performance and fuel economy characteristics. However, they used to be considered as environmentally dirty especially due to the emissions in the form of particulate matter (PM) soot and ash. With the recent developments in combustion and exhaust gas aftertreatment systems, however, PM emissions were remedied so that the reputation of diesel engines is changed significantly. Modern diesel engines are the preferred power source not only for heavy duty applications but also for passenger cars especially in European countries, where fuel economy and greenhouse gases are raising concerns [1].

Diesel engine-sourced PM emissions, which are the inevitable combustion products due to the nature of diffusion combustion, are mainly composed of carbon, hydrocarbons and inorganic compounds. They are in the size range from 20 to 200 nm and can easily penetrate the human body and cause adverse health effects. Diesel particulate filters (DPFs) have been the most effective solution to minimize the PM emissions for the last decade with an efficiency of over 90% [2–8].

DPFs are manufactured from porous materials in a variety of sizes with a range of ceramic materials including SiC,

✉ Nurcan Calis Acikbas
nurcan.acikbas@bilecik.edu.tr

1 Department of Metallurgical and Materials Engineering, Engineering Faculty, Bilecik Seyh Edebali University, 11210 Bilecik, Turkey

2 Department of Mechanical Engineering, Engineering Faculty, Bilecik Seyh Edebali University, 11210 Bilecik, Turkey

3 Department of Chemical and Process Engineering, Engineering Faculty, Bilecik Seyh Edebali University, 11210 Bilecik, Turkey

4 Metallurgy Program, Vocational School, Bilecik Seyh Edebali University, 11210 Bilecik, Turkey

5 TOFAŞ Türk Otomobil Fabrikası A.Ş, Bursa, Turkey

cordierite and aluminum titanate in a wall flow configuration. Filtration is provided by channels of the filter that comprises alternately open and closed ends.

The exhaust gas enters the DPF via the inlet channels passing through the porous wall of the channels. As it passes through the walls, pores of the channel are plugged with accumulated PM, and exhaust gas back pressure increases correspondingly. Therefore, in order to restore the back pressure in the exhaust system, the accumulated PMs must be burned off in certain time intervals, which are called regeneration [9–16]. During the regeneration process, depending on the DPF loading, the temperature can reach to values higher than 1000 °C. In the regeneration process, the particulate burning temperature can be decreased by using a catalyst. The PMs are burned at around 550–650 °C. With a catalyst, the thermo-mechanical stress will not be a crucial factor on the DPF's quality. Such a thermal loading and corresponding thermo-mechanical stresses are the most important parameters for DPF material selection. Thermal shock resistance is the resistance of a brittle material to weakening or fracture subjected to a temperature gradient. Shyam et al. [17] examined the properties that determine the thermal shock resistance of a cordierite DPF. The role of microstructure on the mechanical properties of the filter was discussed in detail. They observed that the coefficient of thermal expansion is the key parameter for the thermal shock resistance. Thermal shock resistance ($R_s = (k * \sigma_f)/(\alpha * E)$) increases with increasing k and $\sigma_f/E\alpha$, where k is thermal conductivity, σ_f is fracture strength, E is elastic modulus and α is linear thermal expansion coefficient. Weibull's statistical maximum risk of rupture criterion states that the flaws existing in a material cause premature failure in strength test. The often observed distribution of strength values in a test is because of the dispersion of flaws in length, shape and density. The risk of rupture increases by the stress amplification near the crack tips. Propagation of preexisting cracks mechanically weakens the DPF material, and even when thermal stresses were not high enough for crack propagation, they constitute additional stresses to mechanical loadings increasing the risk of catastrophic failure. During thermal shock, the increasing crack length causes the necessary temperature difference to drop for crack propagation [18]. The work of She and Ohji [19] showed that after the initial quenching the fracture strength of porous SiC ceramics did not change with further quenching cycles. The results indicated that the crack lengths were out of the critical range for propagation.

Thermal, mechanical and chemical properties of DPFs are mainly controlled by the microstructure of the material. Tailored microstructures and designs can improve the reliability and durability of a DPF. Therefore, characterization of material properties is highly important for cost-effective DPF development and production for outstanding performance characteristics. There are some challenges in characterization and determination of properties of porous materials. Up to date, limited studies are available in the literature on detailed characterization of diesel particle filters [12,17,20–22]. Benaqqa et al. [12] examined thermo-mechanical behavior and phase evolution with increasing temperature as well as the microstructure of SiC DPF. The mechanical and thermal properties in a temperature range up to 1100°C were observed to be stable. It was also emphasized that the durability of any type DPF is strongly dependent on the highly transient thermo-mechanical stresses rather than mechanical fatigue.

In order to determine the fracture toughness, the double-torsion testing methodology was used. Yang et al. [20] examined the basic failures of cordierite DPFs under fleet use conditions. They observed that the failures can be characterized as pinhole, melting, cracking and fouling failures. In order to determine the failures, Yang et al. conducted scanning electron microscope–energy-dispersive X-ray spectroscopy (SEM–EDS), X-ray photoelectron spectroscopy (XPS) and X-ray diffraction (XRD) analyses. They concluded that chemical compositions and crystal structures of the DPF are changed depending on the failure modes. Gordon et. al. [21] examined the fracture toughness of fibrous SiC and mullite materials using the double-torsion test method. It was observed that, due to the microstructural differences, the fracture resistance of fibrous ceramics is much higher than porous monolithic ceramics with similar porosity. It was concluded that the fibrous materials are ideal candidates for DPF applications due to their high porosity and fracture toughness.

To the best of our knowledge, there exist limited studies for characterizations and determination of porous filters' properties in detail. Therefore, in this study macrostructural and microstructural characterizations as well as physical, thermal and mechanical properties identification of a commercial DPF were carried out. The microstructure and the thermal shock parameters were related. The results of this study may prove important especially for the tailoring of the DPF's properties for the thermal shock resistance during the regeneration process.

2 Experimental

The SiC diesel particle filter (DPF) was supplied from TOFAŞ company (Bursa, Turkey). Samples were prepared for microstructural, phase and chemical analysis, mechanical, physical and thermal tests in appropriate size and with standard procedures. Five to ten samples were used for tests and analysis. DPF material was cut in small pieces and ground with a Fritsch Vibrating Cup Mill Pulverisette 9 for 2 min at 900 rpm to obtain powder for X-ray diffraction (XRD), X-ray fluorescence (XRF) and atomic absorption spectroscopy (AAS) analysis. The types of phases of frame-

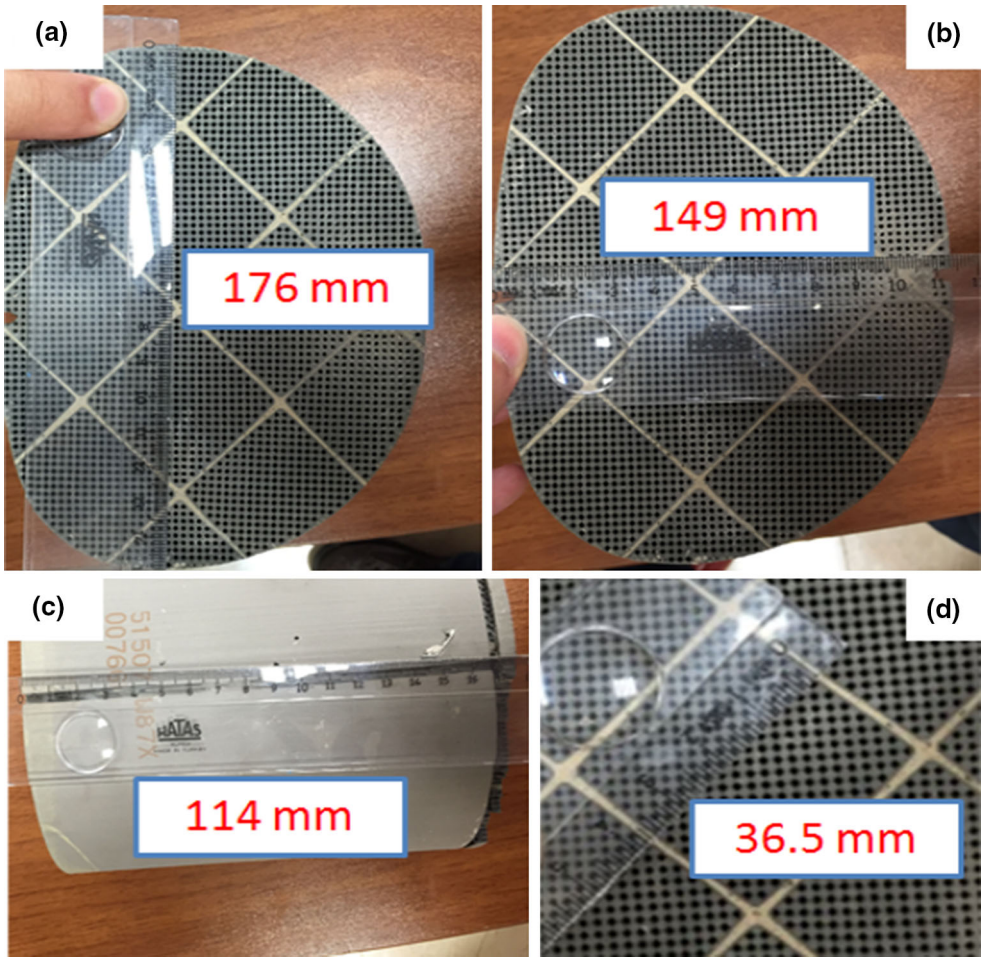

Fig. 1 Dimensions of SiC DPF. **a** Width, **b** length, **c** height, **d** segmented structure

work and grout materials were determined by means of X-ray diffraction analyses (XRD-Panalytical, Empyrean with Cu-Kα radiation). Chemical composition was determined by WD-XRF (Rigaku ZSX Primus model wave length scattering X-ray fluorescence technique). AAS analysis was carried out to determine the metal ion content within DPF (Analytic Jena-ContrAA 300 model AAS).

The Archimedes principle was used to determine the density and porosity of the samples. The samples were submerged in the water and boiled for 2 h on a hot plate at 300 °C. Then, the samples were suspended in water and weighed; also the surface of the samples was dried with tissue paper and weighed. The samples were dried in a furnace at 50–60 °C for 40 min, and their fully dry weights were determined and densities were calculated. Bulk density and a percentage of open porosity values of six DPF samples were calculated using the following equations by using six samples.

$$\text{Bulk Density} = \frac{W_1}{W_3 - W_2} * \rho_{\text{water}} \tag{1}$$

$$\%\,\text{Open Porosity} = \frac{W_3 - W_1}{W_3 - W_2} * 100 \tag{2}$$

where W_1 is dry weight, W_2 is wet weight suspended in water and W_3 is wet weight. The flexural strength and flexural modulus of DPF sample were determined by the three-point bending method with the Shimadzu universal test machine. The crosshead speed was adjusted to 0.7 mm min^{-1}, and the specimen's geometry was prepared according to the ASTM C1674 standard. The calculations were made according to Eqs. 3, 4 and 5.

$$\text{SNB} = \frac{3PL}{2bd^2} \tag{3}$$

$$\varepsilon = \frac{6ds}{L^2} \tag{4}$$

$$E = \frac{1P}{4 \cdot b \cdot s} \cdot \left(\frac{L}{d}\right)^3 \tag{5}$$

where SNB is nominal beam strength, P is breaking force, L is outer (support) span distance, b is specimen width, d is specimen thickness, ε is desired nominal strain rate, s is crosshead rate and E is flexural modulus.

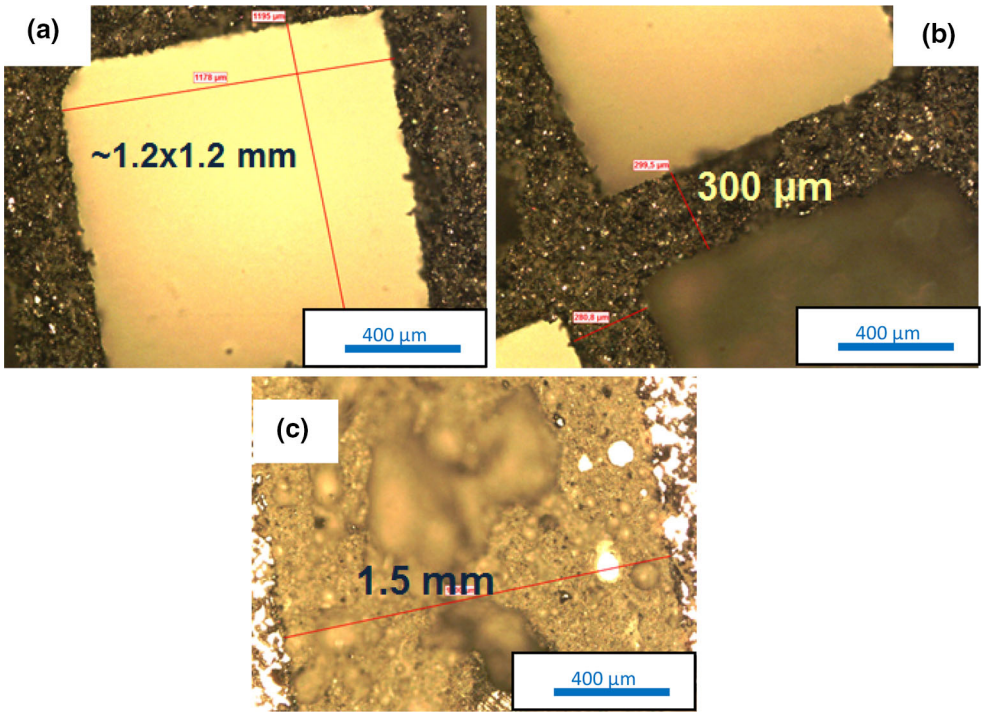

Fig. 2 Optical microscope images of **a** DPF cell, **b** frame thickness between the cells, **c** grout thickness

Optical microscopy (Nikon LV150 model) and scanning electron microscopy (Zeiss Supra 50VP model) was used for macrostructural investigations. FEI Nova NaonoSEM650 with GAD detector was used to obtain high-resolution images with EDX analysis at high voltages (e.g., 20 kV). Especially, GAD detector was used in order to detect Pt/Pd/Au precious metals. Samples were unmounted and unpolished before the SEM-GAD analysis since polishing and/or mounting materials may fill the DPF's pores which is a major challenge in the characterization of this type of porous materials. The GAD detector allowed SEM imaging of an unpolished sample without a conductive coating.

The thermal expansion coefficient (α) was determined with a heating rate of 10 °C min^{-1} up to 1300 °C (Netzsch Dilatometer 402 PC). Thermal conductivity measurements were carried out in two distinct directions (C-Therm thermal conductivity analyzer) at room temperature.

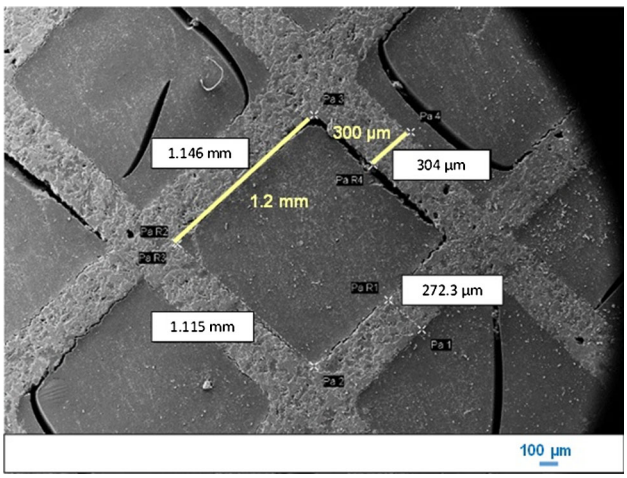

Fig. 3 Top-view SEM-SE image and measurements of frame and edge thickness of DPF

3 Results and Discussion

3.1 Macrostructural Analysis

The macroscopic dimensions of the DPF were determined as 149 × 114 × 176 mm (Fig. 1a–c). The DPF material was manufactured as a segmented structure with a square shape of 36.5 × 36.5 mm (Fig. 1d). It was designed as a ceramic honeycomb substrate structure by extrusion and then combined them together with grout. Each segment was manufactured by extrusion and then combined together with grout. The main reason for the segmented manufacturing of DPFs is the high thermal expansion coefficient of the constituent materials. Otherwise the DPF will be subjected to high thermal stresses which will eventually cause catastrophic failure. However, this manufacturing method causes increased cost. The filter is designed as a wall flow configuration in which one side of the tunnel is open and the other side is closed. Particulate matter will be trapped in the tunnel's wall of the DPF.

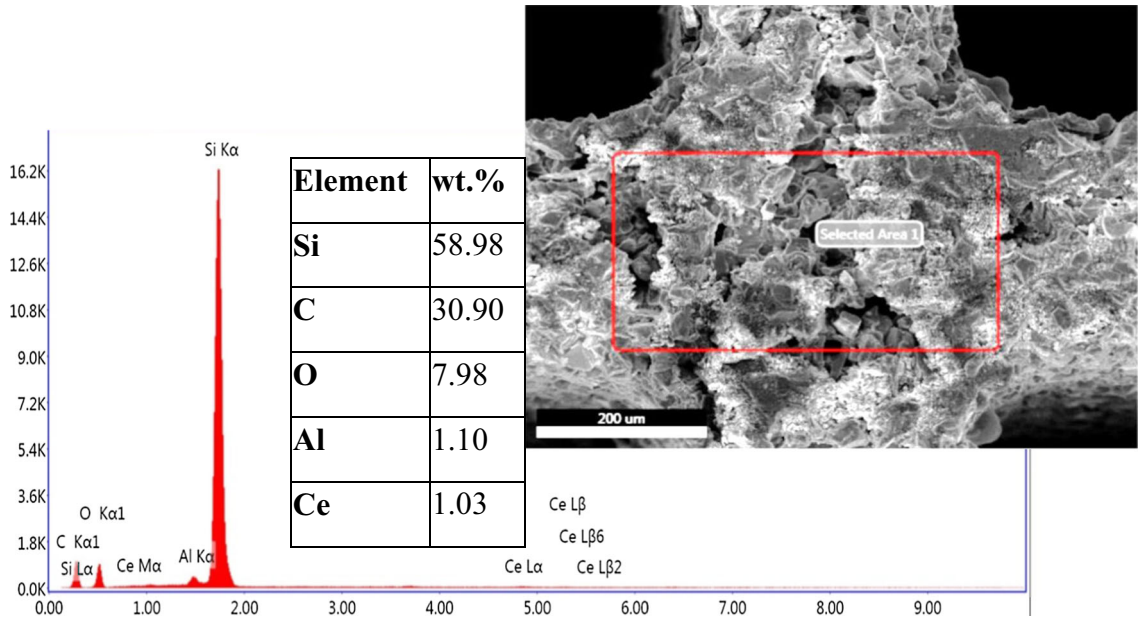

Element	wt.%
Si	58.98
C	30.90
O	7.98
Al	1.10
Ce	1.03

Fig. 4 SEM-EDX analysis result of DPF framework

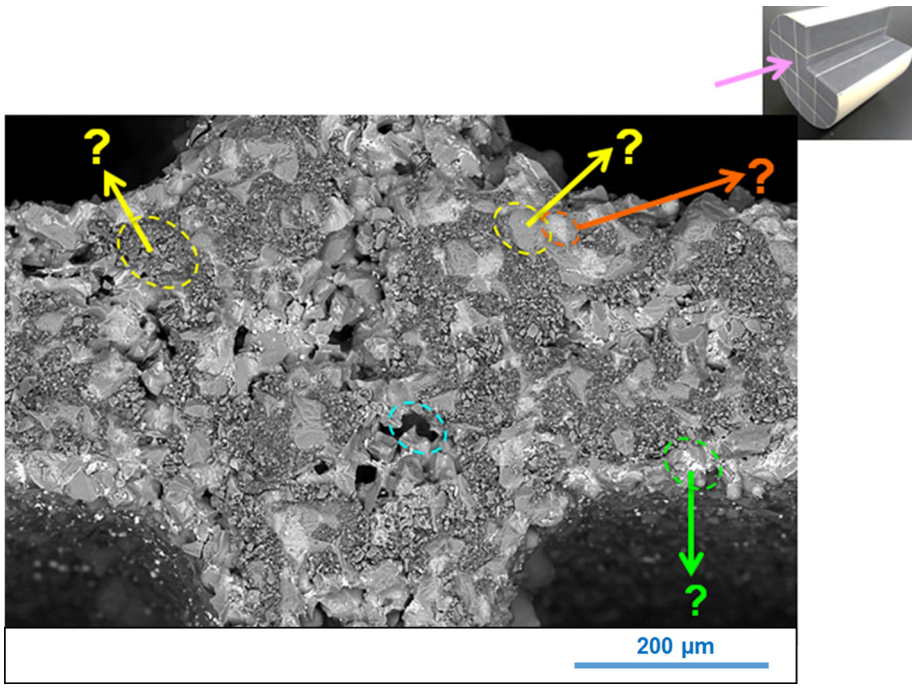

Fig. 5 SEM-BSE image of DPF taken from front side (yellow arrow represent to dark gray grains with fine and coarse structure; red arrow represent the light grains; green arrow represent to white areas; blue dashed line indicates black areas)

A cell size and frame thickness of DPF was measured as ∼ 1.2 × 1.2 mm (Fig. 2a) and ∼ 300 µm (Fig. 2b), respectively. The grout combines the segments of the DPF, and its thickness is 1500 µm (Fig. 2c). The structure of segments was examined also with scanning electron microscopy, secondary electron detector (SEM-SE) at low magnification (100×). The thickness of the skeletal structure and cell size were found as ∼ 300 µm and ∼ 1 mm, respectively (Fig. 3). These results were the same as determined with the optical microscope images.

3.2 Microstructural and Elemental Analysis

In order to determine the chemical composition of the DPF material, EDX analysis was carried out. Silicon and carbon were primary elements with a small amount of oxygen, and

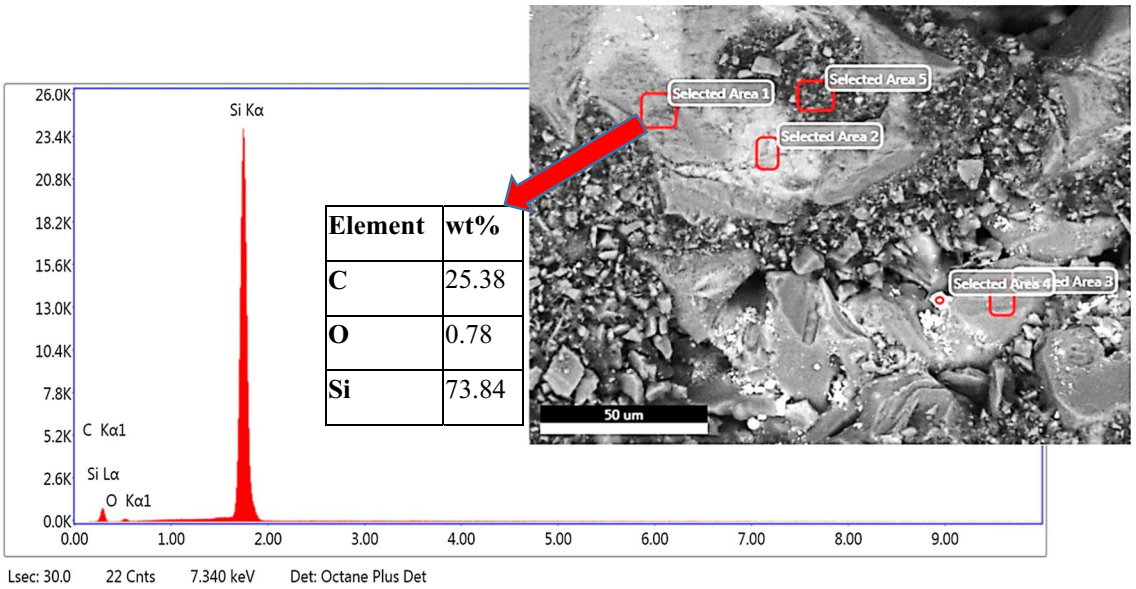

Element	wt%
C	25.38
O	0.78
Si	73.84

Fig. 6 SEM-EDX analysis result of dark gray grains

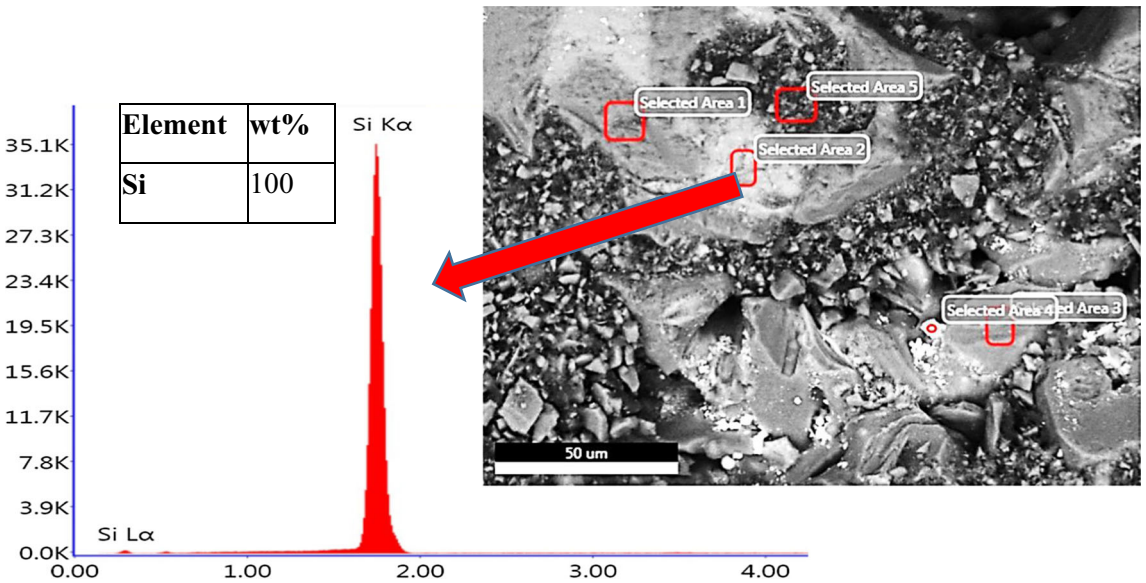

Element	wt%
Si	100

Fig. 7 SEM-EDX analysis result of light gray region

aluminum and cerium were detected (Fig. 4) which suggested that the DPF material is silicon carbide. The presence of aluminum, cerium and oxygen, which could come from catalyst Al_2O_3 and CeO_2, indicated the imparted catalytic function of the filter.

The catalyst is very effective to reduce oxidation temperature of PM accumulated in a DPF. Reducing the oxidation temperature is beneficial for minimizing both the thermal stresses and regeneration fuel, which can be injected to upstream of DPF to burnout the accumulated PM.

A back-scattered electron (BSE) image of the DPF, which was taken from the front side, is given in Fig. 5. The BSE image of the DPF revealed the presence of granular materials with four different contrasting phases which are black, dark and light gray and white. Black regions are pores with size range of 20–50 μm. These pores provide inter-channel flow of exhaust gases.

In addition, the EDX analyses were carried out to determine the composition of these granular materials. EDX analysis of dark gray contrast grains showed that silicon and carbon are the main elements with a low amount of oxygen (Fig. 6). The result suggested that dark gray contrasts grains were SiC which existed in both coarse and fine grain sizes (Fig. 5). The coarse grains were between 10 and 50 μm, and

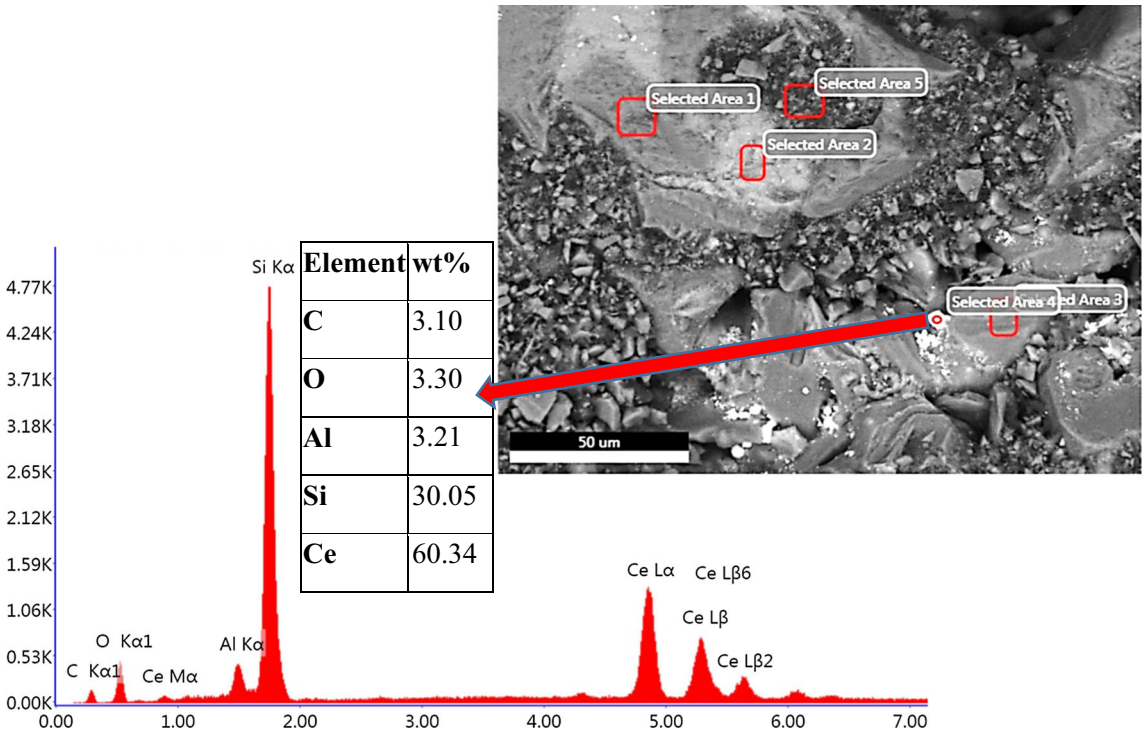

Fig. 8 SEM-EDX point analysis result of white regions

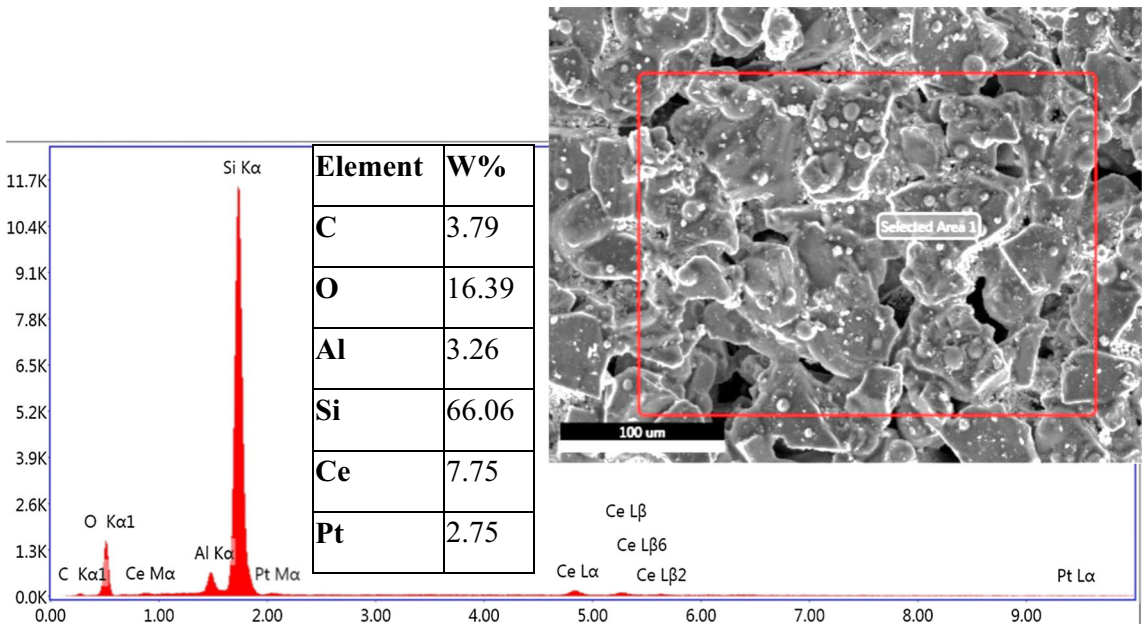

Fig. 9 SEM-EDX area analysis result of DPF along wall

the fine grains were 0.3–1 μm in size. This kind of grain structure provided information that SiC-based DPF was produced with a reaction sintering route. In the method, the capillary effect of the porous medium causes the Si component in the liquid phase to be transported through the pores, and Si reacts with the graphite to form SiC [23,24]. However, the EDX result in the light gray region shown in Fig. 7 as 100 wt% Si suggested an existence of free silicon metal in the system that did not react with graphite. Small white areas were determined as cerium due to strong electron-scattering characteristic of the heavy metals (Fig. 8). Cerium cations were present especially in the walls of the filter providing catalytic effect.

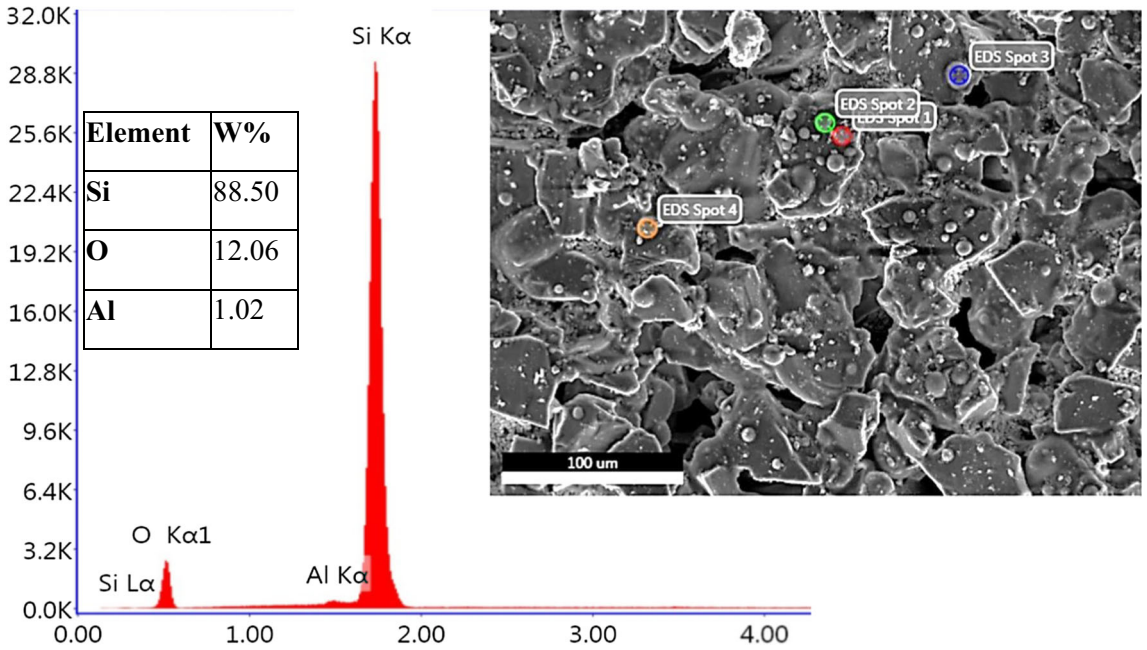

Element	W%
Si	88.50
O	12.06
Al	1.02

Fig. 10 Point EDX analysis result of spherical grains in the wall

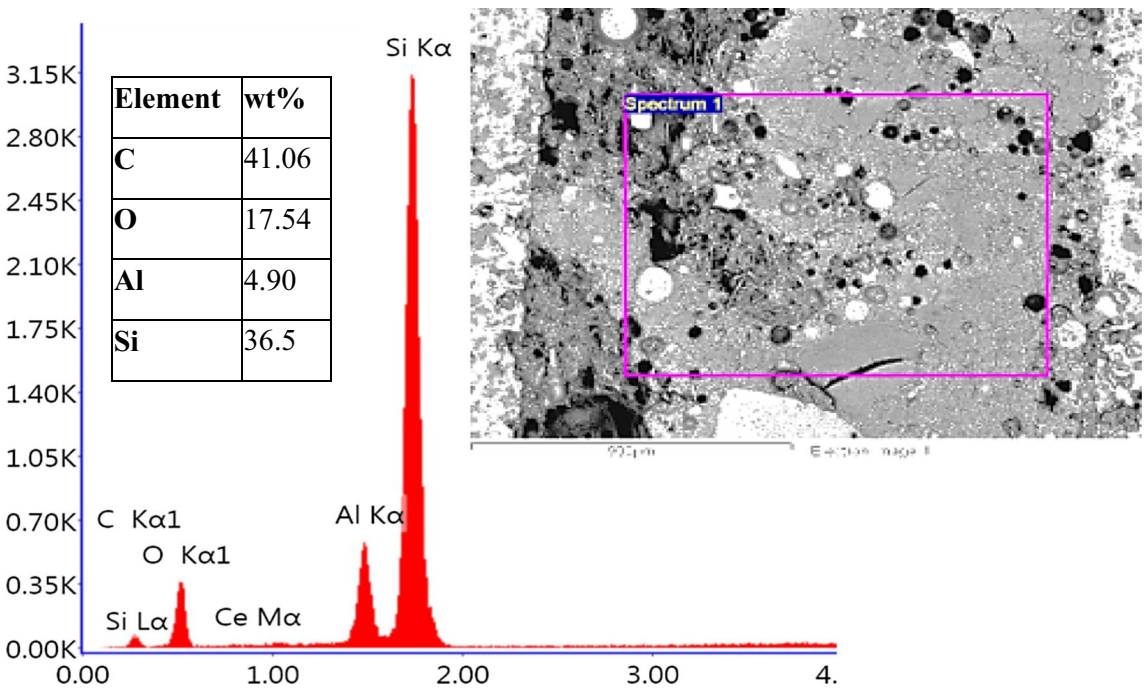

Element	wt%
C	41.06
O	17.54
Al	4.90
Si	36.5

Fig. 11 SEM-EDX analysis result of grout material

The EDX analysis was carried out along the wall where catalytic reactions took place and particles trapped and showed that the primary element was silicon with small amounts of carbon, oxygen, cerium, aluminum and platinum (Fig. 9). The small spherical grains embedded in the larger SiC grains comprised mainly of silicon (Fig. 10). The EDX analysis of the DPF from the front side and along the inner wall provided evidence that the examined DPF segment was produced by a reaction sintering process. However, the presence of unreacted silicon suggested that the sintering process was incomplete.

Grout that was used to combine the separately manufactured segments was investigated by SEM-SE-BSE-EDX detectors (Figs. 11, 12). Grout material was quite porous and

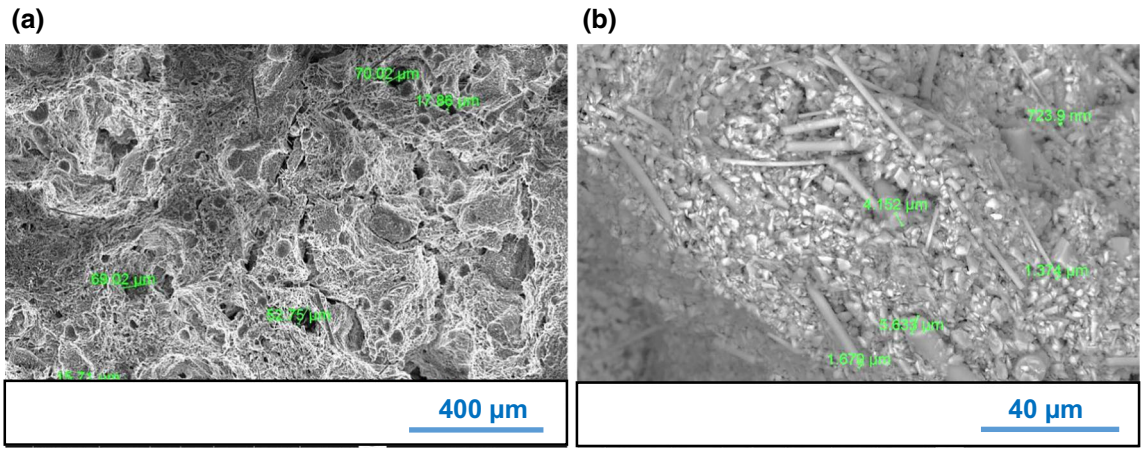

Fig. 12 **a** SE-SEM image and **b** BSE-SEM image of grout material

composed of mainly silicon and carbon with a little amount of oxygen and aluminum. Silicon carbide was the main raw material for the grout. The grout was composed of SiC fibers of diameter between 1 and 6 µm (Fig. 12b). The same composition of the framework and the grout should give rise to low thermo-mechanical stresses during the regeneration process of DPF due to their similar thermal expansion coefficients.

3.3 Phase and Chemical Analysis

The XRD analysis of the framework and the grout showed that both of them had similar composition but with different quantities. Main phase was silicon carbide of different polymorphs (15R, 6H, 4H), and silicon and crystobalite peaks were available (Fig. 13). Among the SiC polytypes, 6H (hexagonal SiC) is the most commonly occurring modification in commercial SiC. The next most common polytypes are 15R (rhombohedral crystal structure) and 4H, respectively. The hexagonal and rhombohedral polytypes are sixfold symmetry axis along the stacking direction (*c*-axis) and hence show anisotropic properties. Silicon and crystobalite peak intensities were greater for the framework than for the grout. The XRD results (SiC + Si) also provided evidence that the DPF part was produced by the reaction sintering method.

XRF analysis of the framework showed that main elements were silicon (92.91 wt%.) with low amounts of cerium (3.63 wt%) and aluminum (3.46 wt%). Carbon and oxygen elements were not detected with the XRF due to their low atomic weight and instrument calibration set up. The precious metal, platinum, was dispersed on the surface and within the pores of the washcoat layer that was composed of aluminum oxide and cerium oxide. AAS (atomic absorption spectroscopy) was used to determine the Pt content as 0.045 wt% of the washcoat layer. The Pt catalyst deposited within the washcoat functions as catalyst in contact with the exhaust gas flowing through the channels for its catalytic conversion.

3.4 Physical Properties

Essential function of the DPF was the filtering of the particle matters after the burning of the diesel fuel with its porous structure. Therefore, open porosity percentage and pore size distribution were the most important parameters for DPF efficiency. Bulk density and % open porosity as determined by the Archimedes principle were found to be 1.97 g cm^{-3} and 30%, respectively. The starting raw material properties (composition, particle size, particle size distribution), production method (such as solid-state sintering and liquid-phase sintering) and conditions (sintering temperature and duration and the use of gasifying pore formers) all determined the final porosity and pore structure [25]. In order to determine the pore size, detailed SEM-SE images of the wall of the filter were taken from different parts. The pore sizes were determined to change between 10 and 50 µm (Fig. 14) by the 10 SEM-SE images which were taken from random areas over the entire filter surface. Approximately 150 measurements were carried out in order to determine the mean pore size to be 20–25 µm. In the literature, it is known that 20- to 25-micron pore size filters are used with 80–90% efficiency [4].

3.5 Mechanical and Thermal Properties

Stress–strain curve of the porous SiC material is given in Fig. 15. The flexural strength and elastic modulus of the DPF with 30% porosity were found as 16.27 MPa and 7.3 GPa, respectively. The most important parameter affecting the value of flexural strength was the porosity for SiC ceramic filters. In the literature, different samples with diverse porosity levels (9–91%) yielded a wide range of flexural strength values (0.7–205 MPa) [4,12,26].

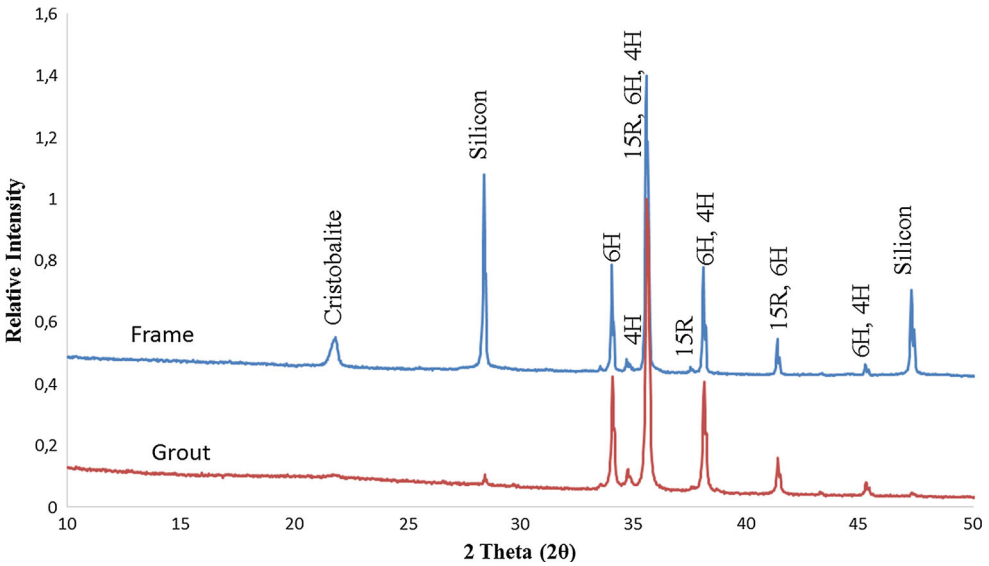

Fig. 13 The XRD analysis of framework and grout

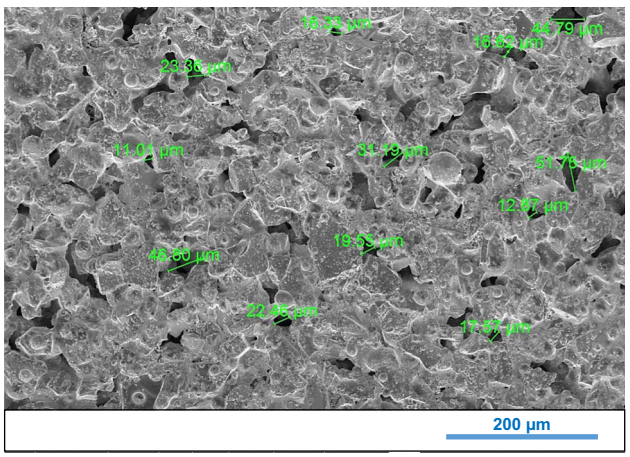

Fig. 14 Representative SEM-SE image and porosity size measurements of sample through DPF wall

Thermal conductivity (k) values were measured in different directions (x and y). x was taken as the direction of the DPF walls, while y direction passes through the frame and channels. The results obtained in the x and y directions were 2.125 and 1.775 W/mK, respectively, and the mean value of thermal conductivity was calculated as 1.95 W/mK. The measured values of the thermal conductivity of the porous sample and fully dense SiC (∼ 120 W/mK) were totally different due to the decreasing thermal conductivity with increasing porosity. The thermal expansion coefficient (α) of SiC filter in the temperature range of 700–1300 °C was found to be $5.23 \times 10^{-6}\,K^{-1}$ (Fig. 16) close to the literature values [12]. The thermal expansion coefficient value changes between 5.01 and 5.04 $\times 10^{-6}\,K^{-1}$ in the temperature between 200 and 450 °C. Between 450 and 1300 °C, the value is around 5.27×10^{-6} K. These thermal expansion coefficient values

Fig. 15 Stress–strain curve of porous SiC DPF

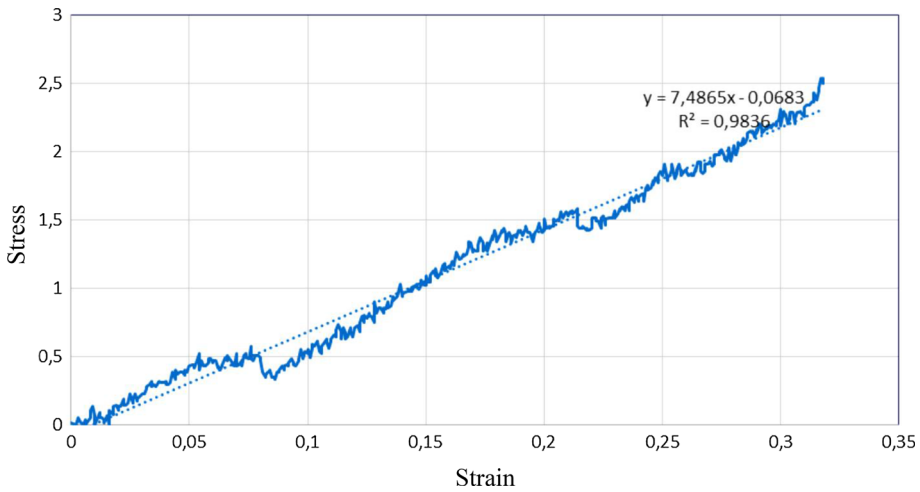

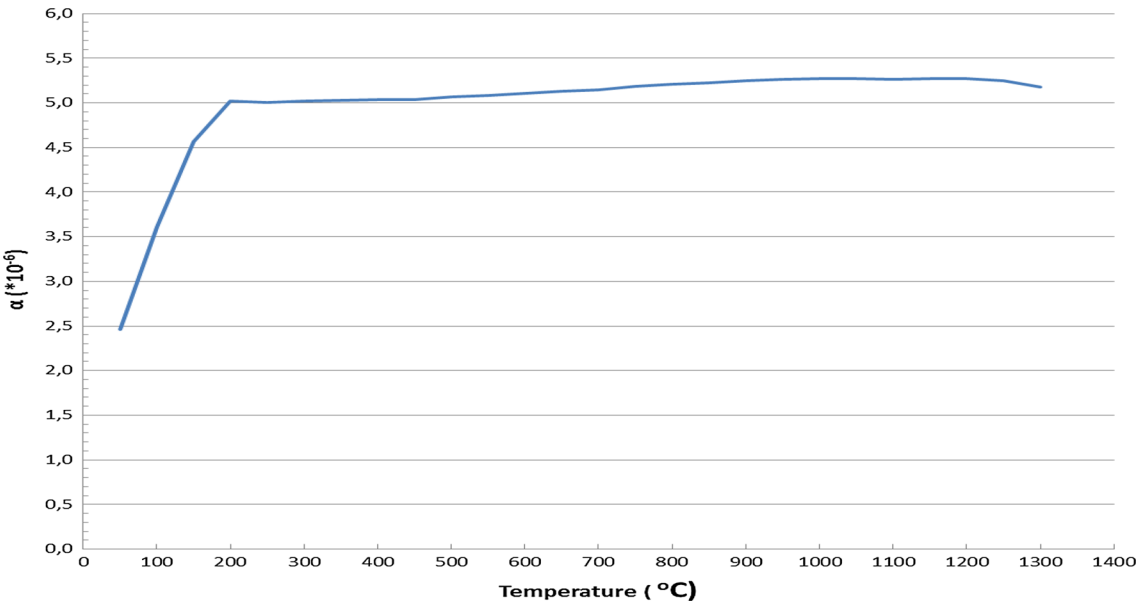

Fig. 16 Thermal expansion versus temperature graph of SiC DPF

indicated the stability of SiC DPF in the investigated temperature range.

The value of the thermal shock resistance ($R_s = (k * \sigma_f)/(\alpha * E)$) parameter group $\sigma_f/E\alpha$ was calculated to be 426 K, while k was 1.95 W/mK. When compared to the literature values for dense SiC ($\sigma_f/E\alpha$ 550 $\times$ 10^6 Pa/410 $\times$ 10^9 Pa/4.0 $\times$ 10^{-6} K^{-1} = 335 K, k was 120 W/mK), thermal shock resistance due to the parameter group $\sigma_f/E\alpha$ was better; however, thermal conductivity was an order of magnitude lower making the thermal shock resistance worse. Therefore, for better thermal shock resistance of the filter material, thermal conductivity value has to be increased as much can be allowed by the required porosity as possible. Thermal conductivity may be increased by tailoring the microstructure with elongated and aligned grain structure for better thermal shock resistance.

4 Conclusions

In this study, the characterization of a commercial DPF material was carried out with different techniques with the aim of identification of the manufacturing processes, determination of the chemical composition, microstructure, mechanical, physical and thermal properties. Following conclusions were reached:

- The framework and grout were produced from SiC powder, shaped with extrusion in segmented structure and densified by the reaction sintering process. The size of the square-shaped segments was $\sim$ 36.5 mm. It comprised open and closed cells of $\sim$ 1.2 $\times$ 1.2 mm in size with porous walls allowing exhaust gas flow. Grout thickness between the segments was $\sim$ 300 μm.
- Microstructural evaluation revealed that the DPF framework consisted of pores in the range of $\sim$ 10–50 μm in size, coarse and fine SiC grains of size 10–50 μm and 0.3–1 μm, respectively, and coarse silicon grains with 10–30 μm.
- Chemical analysis results showed that SiC substrate was coated with a mixture of CeO_2–Al_2O_3 as the washcoat layer within which nano sized Pt was homogeneously dispersed.
- Phase analysis and chemical analysis results revealed that framework and grout had similar chemical composition (SiC, Si and SiO_2).
- Physical test showed that open porosity was 30%. Flexural strength and modulus were found as 16.27 MPa and 7.36 GPa, respectively. Room temperature thermal conductivity value was 1.95 W/mK, and thermal expansion coefficient between 500 and 1300 °C was 5.23 $\times$ 10^{-6} $°C^{-1}$. The value of the thermal shock resistance parameter group $\sigma_f/E\alpha$ was calculated to be 426 K. When compared to the literature values for dense SiC ($\sigma_f/E\alpha$ = 335 K, k was 120 W/mK), thermal shock resistance due to the parameter group $\sigma_f/E\alpha$ was better; however, thermal conductivity was an order of magnitude lower, causing a decrease in the thermal shock resistance. Thermal conductivity may be increased by tailoring the microstructure with elongated and aligned grain structure for better thermal shock resistance.

Acknowledgements This work was financially supported by Bilecik Seyh Edebali University Scientific Research Projects (Project Nos. 2015-02.BŞEÜ.03-07 and 2016-01.BŞEÜ.03-01).

References

1. Adler, J.; Petasch, U.: Handbook of Advanced Ceramics: Chapter 8.1. Diesel Particulate Filters. Elsevier Inc. Chapters, Amsterdam (2013)
2. Liati, A.; Eggenschwiler, P.D.; Gubler, E.M.; Schreiber, D.; Aguirre, M.: Investigation of diesel ash particulate matter: a scanning electron microscope and transmission electron microscope study. Atmos. Environ. **49**, 391–402 (2012)
3. Saint-Georges, F.; Garcon, G.; Escande, F.; Abbas, I.; Verdin, A.; Gosset, P.; Mulliez, P.; Shirali, P.: Role of air pollution particulate matter (PM2.5) in the occurrence of loss of heterozygosity in multiple critical regions of 3p chromosome in human epithelial lung cells (L132). Toxicol. Lett. **187**, 172–179 (2009)
4. Adler, J.: Ceramic diesel particulate filters. Int. J. Appl. Ceram. Technol. **2**(6), 429–439 (2005)
5. Yang, J.; Stewart, M.; Maupin, G.; Herling, D.; Zelenyuk, A.: Single wall diesel particulate filter (DPF) filtration efficiency studies using laboratory generated particles. Chem. Eng. Sci. **64**, 1625–1634 (2009)
6. Choi, H.J.; Kim, J.U.; Kim, S.H.; Lee, M.H.: Preparation of granular ceramic filter and prediction of its collection efficiency. Aerosolsci. Technol. **48**, 1070–1079 (2014)
7. Alvin, M.A.: Advanced ceramic materials for use in high temperature particulate removal systems. Ind. Eng. Chem. Res. **35**, 3384–3398 (1996)
8. Soylu, S.: Development of PN emission factors for the real world urban driving conditions of a Hybrid City Bus. Appl. Energy **138**, 488–495 (2015)
9. Nemoto, A.; Iwasaki, K.; Yamanishi, O.; Tsuchimoto, K.; Uoe, K.; Toma, T.; Yoshino, H.: Development of Innovative Diesel Particulate Filters Based on Aluminum Titanate: Design and Validation, pp. 1–11. Sumitomo Kagaku, Chūō (2011)
10. Eggenschwiler, P.D.; Schreiber, D.; Liati, A.: Active regeneration characteristics in diesel particulate filters. In: SAE Technical Paper, 24-0185 (2011)
11. Chi, H.; Ji, Z.; Sun, D.; Cui, L.: Experimental investigation of dust deposit within ceramic filter medium during filtration-cleaning cycles. Chin. J. Chem. Eng. **17**, 219–225 (2009)
12. Benaqqa, C.; Gomina, M.; Beurotte, A.; Boussuge, M.; Delattre, B.; Pajot, K.; Pawlak, E.; Rodrigues, F.: Morphology, physical, thermal and mechanical properties of the constitutive materials of diesel particulate filters. Appl. Therm. Eng. **62**, 599–606 (2014)
13. Shyam, A.; Lara-Curzio, E.; Watkins, T.R.; Parten, R.J.: Mechanical characterization of diesel particulate filter substrates. J. Am. Soc. **91**, 1995–2001 (2008)
14. Freitas, N.L.D.; Gonçalve, J.A.S.; Innocentini, M.D.M.; Coury, J.R.: Development of a double-layered ceramic filter for aerosol filtration at high temperatures: the filter collection efficiency. J. Hazard. Mater. **136**, 747–756 (2006)
15. Fino, D.: Diesel emission control: catalytic filters for particulate removal. Sci. Technol. Adv. Mater. **8**, 93–100 (2007)
16. Tsuneyoshi, K.; Yamamoto, K.: A study on the cell structure and the performances of wall-flow diesel particulate filter. Energy **48**, 492–499 (2012)
17. Shyam, A.; Lara-Curzio, E.; Pandey, A.; Watkins, T.R.; More, K.L.: The thermal expansion, elastic and fracture properties of porous cordierite at elevated temperatures. J. Am. Ceram. Soc. **95**(5), 1682–1691 (2012)
18. Ozcan, S.; Tran, H.: Evaluation of the effectiveness of the bulk thermal stresses for kraft recovery boiler fireside deposit cleaning. Tappi J. **5**(4), 3–9 (2006)
19. She, J.; Ohji, T.: Thermal shock behavior of porous silicon carbide ceramics. J. Am. Ceram. Soc. **85**(8), 2125–27 (2002)
20. Yang, K.; Fox, J.T.; Hunsicker, R.: Characterizing diesel particulate filter failure during commercial fleet use due to pinholes, melting, cracking, and fouling. Emiss. Control Sci. Technol. **2**, 145–155 (2016)
21. Gordon, T.; Shyam, A.; Lara-Curzio, E.: The relataionship between microstructure and fracture toughness for fibrous materials for diesel particulate filters. J. Am. Ceram. Soc. **93**(4), 1120–1126 (2010)
22. Gurlek, E.: Characterization of Diesel Particle Filter. M.Sc. Thesis. Bilecik Seyh Edebali University, Bilecik (2016)
23. Ness, J.N.; Page, T.F.: Microstructural evolution in reaction-bonded silicon carbide. J. Mater. Sci. **21**, 1377 (1986)
24. Paik, U.; Park, H.C.; Choi, S.C.; Ha, C.G.; Kim, J.W.; Jung, Y.G.: Effect of particle dispersion on microstructure and strength of reaction-bonded silicon carbide. Mater. Sci. Eng. A **334**(1–2), 267–274 (2002)
25. Studart, A.R.; Gonzenbach, U.T.; Tervoort, E.L.; Gauckler, J.: Processing routes to macroporous ceramics: a review. J. Am. Ceram. Soc. **89**, 1771–1789 (2006)
26. Eom, J.H.; Kim, Y.W.; Raju, S.: Processing and properties of macroporous silicon carbide ceramics: a review. J. Asian Ceram. Soc. **1**, 220–242 (2013)